Published by
NIGERIAN SOCIETY OF PHYSICAL SCIENCES
Available online @ https://asr.nsps.org.ng/index.php/asr

African Scientific Reports 3 (2025) 225

African Scientific Reports

Synthesis and characterization of ZnO crystalline powder: effect on Alkaline pH

A. A. Ibiyemi[a,*], J. I. Lawal[a], A. Adewole[a], A. F. Ojo[a], S. K. Aminu[a], G. O. Ogunyemi[a], A. S. Olatunde[a], A. O. Ogungbe[a], A. T. Oladimeji[a], T. I. Ogunniran[a], M. T. Olatunji[a], I. E. Olaoye[a], O. P. Oladipo[a], B. M. Akinroye[a,b], A. C. Adeniran[b]

[a] *Department of Physics, Federal University, Oye-Ekiti, Nigeria*
[b] *Department of Physics, Osun State College of Technology, Esa Oke, Nigeria*

Abstract

Zinc Oxide nanoparticles (ZnO NPs) were effectively produced using the co-precipitation method in alkaline solutions with pH values of 8, 10, and 12. The X-ray diffraction (XRD) investigation indicates that the preferred orientation for the formation of ZnO phase and wurtzite-hexagonal structure is the (101) reflection plane. The crystallite size of ZnO produced at pH 8, 10 and 12 are 19.74 nm, 14.83 nm and 8.64 nm, respectively. The scanning electron microscope (SEM) result revealed spongy-like morphology and spherical grains nanostructure at all pH level. XRD analysis demonstrated that the hexagonal wurtzite structure is present in the ZnO nanostructure. The energy band gap is decreased with increasing pH. The smooth and uniform shape of sample synthesized at pH 12 with large-scale homogeneity is an important point, this suggests that these nanoparticles may be useful for photodetectors. Because of its high optical gain, the ZnO NPs synthesized at pH 8 exhibits the best optical characteristics, whereas the ZnO NPs created at pH 12 exhibits optical losses for optoelectronics device application. This work has shown that altering the precursor's pH altered the zinc oxide sample for a range of industrial uses. For example, using pH 12 greatly raised the absorbance value, showing that ZnO is a promising photovoltaic (PV) material and ultraviolet (UV) detector since its light absorption is much boosted at high pH values. Meanwhile, the addition pH 8 greatly raised the transmittance value, demonstrating that ZnO's visible light transparency is significantly enhanced at low pH levels in alkaline medium, making it a potential optoelectronics material and active infrared detector. According to the study's findings, ZnO NPs has use in photovoltaic materials, optoelectronics, and UV and infrared detectors.

DOI:10.46481/asr.2025.4.2.225

Keywords: Optoelectronics, pH, Transmittance, Absorbance, ZnO

Article History :
Received: 07 August 2025
Received in revised form: 15 April 2025
Accepted for publication: 03 May 2025
Published: 31 May 2025

1. Introduction

Numerous conventional and non-commercial energy sources are used to supply the world's energy needs. Although there are now more industrial energy sources, huge amount of the energy in rural regions still comes from fuel wood. In addition to being ineffective for final use, using green wood as fuel has a detrimental impact on the environment and increases pollutants [1]. Utilizing renewable

---

[*] Corresponding author Tel. No: +234-806-219-8624.
Email address: `abideen.ibiyemi@fuoye.edu.ng` (A. A. Ibiyemi)

energy sources, particularly photovoltaic solar energy, which is plentiful and has a long lifespan, can help attain sustainable energy. Photovoltaic is a primary method of converting solar energy to electricity [2]. The capacity of photovoltaic (PV) solar cells to directly convert solar energy into electrical power has been the subject of research for the past three decades. In urban settings, photovoltaic energy conversion provides a silent, emission-free method of producing electricity. Renewable energy sources, particularly solar energy [3], which is abundant and has a long usable life, can be used to generate sustainable energy. For three decades, researchers have been investigating the use of PV systems to generate solar electricity [4]. Even now, these sources are still a long way from being profitable.

In PV system one essential energy source is the sun, and solar radiation is the powerful energy that the sun emits, especially electromagnetic energy. The visible portion of the electromagnetic spectrum makes up larger portion of it, with the remaining portion primarily located in the ultraviolet (UV) and near-infrared (NIR) regions. The finest technological method for capturing and turning solar radiation into power is a solar PV system. Having a solar PV system that is long-lasting and has a higher conversion efficiency in the previously indicated electromagnetic spectrum is crucial. To do this, a semiconductor material with an energy band gap between 1.5 and 3.0 eV that can be supplied locally and is reasonably priced is needed. Many contemporary technologies, including optoelectronics, sensing, and computing rely heavily on semiconductors due to their excellent properties and capabilities that can be applied to optoelectronic devices. Wide band gap oxide semiconductors such as zinc oxide are a unique class of materials that combine superior optical transparency and electrical conductivity [5]. Because of their plentiful optical transparency, electrical conductivity that can be tuned, and adjustable carrier concentration, wide band gap oxide materials are crucial for both new and modern electronic devices and energy applications. Because of their characteristics, they are widely used as primary materials in optoelectronic device applications. Wide band gap semiconductors that are of very important research interest are transparent conductive oxides (TCOs), like amorphous ZnO NPs, utilized in displays, optoelectronic and, solar cells. ZnO nanostructure semiconductors, in particular, have attractive building blocks for device application in energy conservation coating materials for window glasses, solar cells, etc. In recent years, metallic oxide semiconductors have been observed to exhibit tremendous tuning characteristics that guarantee their usage in many scientific fields. It is crucial to alter the optical energy band gap in order to utilize this material for PV and other applications. However, as far as we know, there isn't a current publication available that focuses on the pH effect of zinc oxide in alkaline medium using co-precipitation technique for photo sensing and photovoltaic device application. The morphology of the materials was used to investigate the photosensing device application of ZnO.

Among the II-VI semiconductor family, ZnO NPs is one of the most promising chemical and is a wide direct energy band-gap material [6, 7]. Because of its direct energy band-gap with huge excitonic binding energy, optoelectronics may find use for it [8]. Additionally, ZnO has a high radiation resistance [9], making it a good material for gas sensors [10], piezoelectric transducers, photodiodes, and photo-detectors [8]. ZnO often crystallizes in the wurtzite crystal form with the existence of tetrahedral coordination allying with four oxygen atoms and one zinc atom inside the wurtzite structure. Since the real structure of chemically synthesized ZnO NPs may differ slightly from the ideal wurtzite structure, the c/a ratio is typically found to be less than 1.633 [11]. The lattice constants of the wurtzite structure are a = 3.25 Å and c = 5.21 Å, respectively, and it has a hexagonal unit cell. The lattice constant ratio (c/a) for the optimal structure is found to be approximately 1.633 [11].

To create ZnO NPs, various synthesis techniques could be applied [12, 13]. Additionally, many nanostructures of ZnO may be generated [14], and each of these nanostructures has distinct optical characteristics. ZnO is also a non-toxic substance, which is why medication delivery to diseased parts of the body has been accomplished using ZnO [14]. ZnO have also been utilized to catalyze chemical processes [12, 13]. Thus, it is crucial to conduct research on the synthesis of ZnO NPs with precise size and form using appropriate chemical synthesis methods. According to earlier research, the morphology of the synthesized metal oxide nanoparticles is signifcantly dependent on the amount of H^+ or OH^- ions present in the precursor [15]. The metal-oxygen bond polymerization during the zinc oxide development process is determined by the aforementioned ions [16]. As a result, changes in the solution's pH have a significant impact on the hydrolysis and condensation reactions that take place during the creation of the precursor solution [17]. The shape and optical characteristics of biosynthesized nanoparticles are further influenced by this pH difference [18].

ZnO NPs were produced in this work using a commonly utilized and straightforward co-precipitation process. The bottom-up method is the foundation of the co-precipitation synthesis methodology, which is used to create nanostructures [19]. The product yield by this method is minimal, and the finished product might include some unreacted raw components or contaminants. As a result, it is required to repeatedly wash the finished object with alcohol or distilled water. Nonetheless, this straightforward method is highly helpful for doping semiconductor nano-crystals with other elements and synthesizing control nanostructure, or size and shape. ZnO NPs has the potential to be substituted with conventional thin layered conductive indium tin oxide due to its optical transparency to visible light [11]. The conditions during processing and the synthesis procedure are typically what determine the characteristics of ZnO NPs. In this work, we present the summary of ZnO nanostructures utilizing the co-precipitation process at different pH levels. Subsequently, this work presents the optical, morphological and structural characterization of ZnO NPs.

2. Methodology

Figure 1 illustrates the schematic diagram of the experimental procedure of ZnO nanoparticles. The starting components for the current study are ammonia (NH_3) solution, sodium hydroxide (NaOH), and zinc chloride (ZnCl). ZnO NPs were created using the

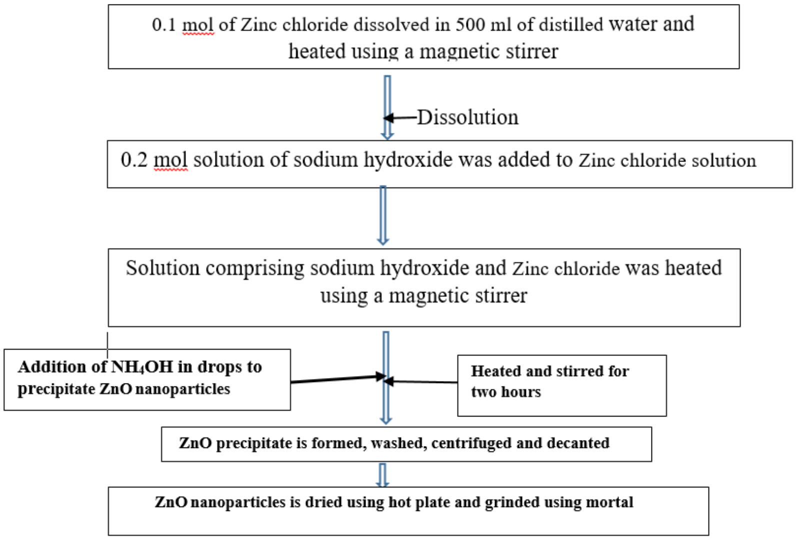

Figure 1. Schematic diagram of experimental procedure of zinc oxide nanoparticles.

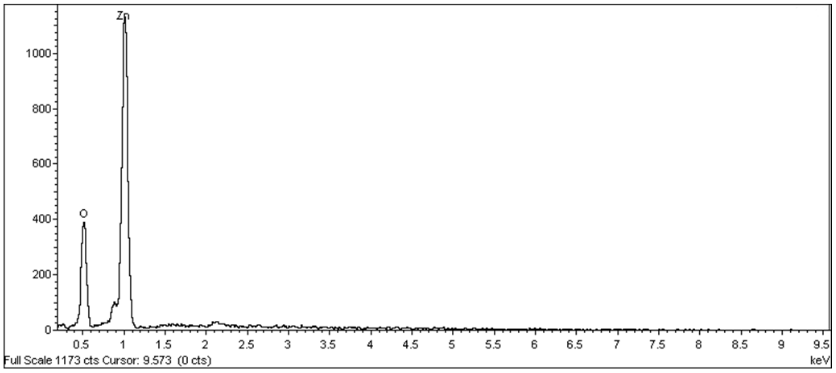

Figure 2. Spectral showing the Energy Dispersive X-ray Spectroscopy of ZnO sample.

chemical co-precipitation method. Zinc chloride (ZnCl) and sodium hydroxide (NaOH) in an aqueous solution in deionized water were combined to create the solution medium. Using a computerized weighing balance, the necessary weight of the compounds' aqueous solution was calculated. 0.1 mol of Zinc chloride were dissolved in 500 ml of distilled water and heated using a magnetic stirrer. The solution was then kept under constant stirring to completely dissolve zinc chloride for one hour. After full dissolution of zinc chloride, 0.2 mol solution of sodium hydroxide was added which was then constantly stirred. The reaction was allowed to proceed for 2 hours after complete addition of ammonia solution and the attainment of required pH values (8, 10 and 12). Drop by drop, ammonia solution was added until pH values of 8, 10, and 12 were reached, which helps the precipitate to form. The solution was centrifuged for 10 min and the supernatant was discarded. After removing undesired particles by washing with deionized water, the precipitated nanoparticles were dried on a hot plate. The samples of nanoparticles were ground to produce fine particles in powdery form.

2.1. Sample characterization

The optical properties such as transmittance and absorbance of the nanoparticles were examined using UV–Vis spectrophotometer (Jasco-V-570 Spectrophotometer, Japan), surface morphology were examined using Scanning Electron Microscope (FEG JEOL JSM-7800). The structural characteristics were examined by employing X-ray diffraction technique (Rigaku powder X-ray Diffractometer Ruker Advanced D8 model with CuK α radiation λ = 1.5406 Å) and the atomic composition were formed using Energy Dispersive X-ray Spectroscopy (Quantax 200 with X Flash e Bruker).

Table 1. ZnO nanoparticle crystallite sizes and lattice constants obtained at various pH levels.

H	Crystallite size D (nm)	Lattice parameter a (Å)	Lattice parameter c (Å)	X-ray density dX (g/m^3)	Porosity (%)	Dislocation density (lines/m^2)	micro strain (ε)
8	19.74	3.2553	5.2245	5.64	14.185	0.00256	0.0547
10	14.83	3.2625	5.2283	3.76	21.657	0.00455	0.0276
12	8.64	3.2656	5.2312	2.95	45.747	0.01067	0.0196

Table 2. ZnO nanoparticle d-spacing for each diffraction peak.

2-theta	d-spacing	lattice plane
31.698	2.8205	(1,0,0)
34. 356	2.6081	(0,0,2)
36.184	2.4804	(1,0,1)
47.461	1.9141	(1,0,2)
56.529	1.6266	(1,1,0)
62.791	1.4786	(1,0,3)
66. 305	1.4085	(2,0,0)
67.876	1.3797	(1,1,2)
69.015	1.3596	(2,0,1)
72.503	1.3026	(0,0,4)
76.899	1.2387	(2,0,2)
81.324	1.1821	(1,0,4)
89.537	1.0938	(2,0,3)
92.708	1.0645	(2,1,0)
95.248	1.0427	(2,1,1)
98.568	1.0163	(1,1,4)

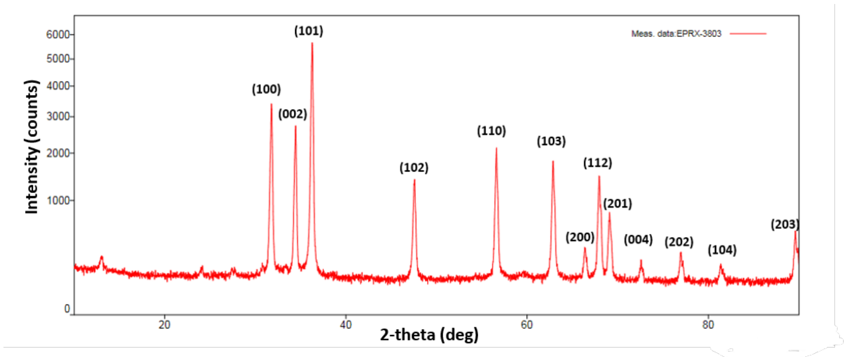

Figure 3. Diffraction pattern of ZnO NPs synthesized using pH 8.

3. Results

3.1. Elemental Dispersive Spectroscopy

Elemental Dispersive X-ray Spectroscopy (EDS) was used to determine the elemental composition of the produced compounds. Figure 2 shows the EDS spectra of the compound that were produced. Elemental dispersive X-ray spectroscopy (EDX), a popular analytical method, was used for the elemental examination of samples. EDX spectra of the obtained pure samples were used to determine their chemical composition. Zn and O are the only elementary species found in the sample. The binding energies of Zn are linked to the peaks at 1.0 Kev in addition to the oxygen (O) peak at 0.5 Kev. Thus, in pure samples, EDX showed that the nanoparticles included both zinc and oxygen. In both samples, there are no other peaks that relate to any other elements. As a result, the processed items are regarded as pure and free of contamination. Zn^{2+} is a member of the L-series of energy spectra, while O^{2-} belong to the K-series of energy spectra. The synthetic nanoparticles are 100% pure, as demonstrated by the EDS's detection of no foreign elements (impurities). A percentage of the elements have been discovered to have excess zinc, and the pertinent findings are in agreement with XRD diffraction analysis.

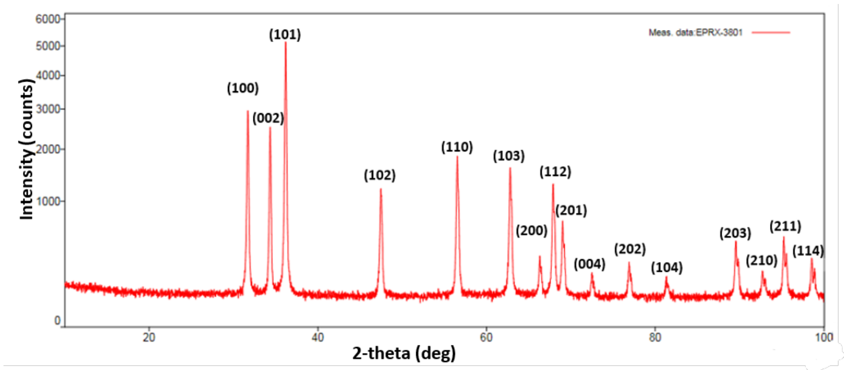

Figure 4. Diffraction pattern of ZnO NPs synthesized using pH 10.

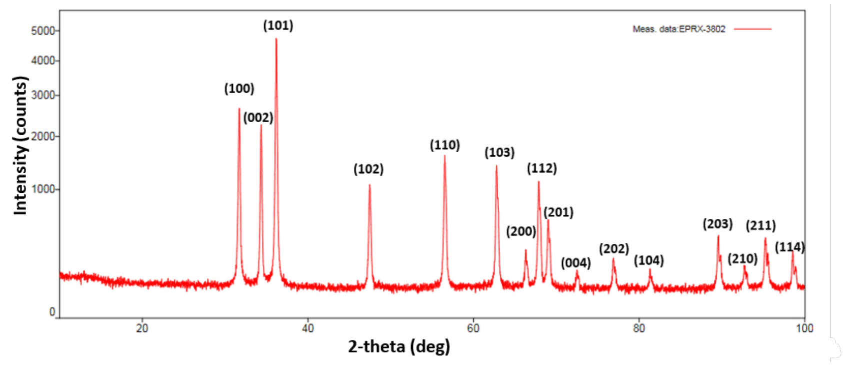

Figure 5. Diffraction pattern of ZnO NPs synthesized using pH 12.

3.2. *X-ray diffraction*

Using a step size of 0.02°, the sample was scanned at a diffraction angle of 2θ from 0° to 80°. Thus, for pH 8, pH 10 and pH 12, the XRD profiles of ZnO NPs were obtained and are displayed in Figures 3-5. According to the pattern, ZnO NPs with varying pH are composed of hexagonal wurtzite structure with a preferred orientation of diffraction plane (101). The ZnO NPs characteristic line broadened and their crystalline structure was display in the XRD patterns. The three most resilient lines in a typical XRD pattern for a hexagonal structure are found at a 2θ value of 31.698-36.184. Diffraction peaks are consistent with the ZnO phase of Powder Diffraction File card database No. 01089-0510. The decrease in the crystallite size as pH increases is govern by the broadening of the diffraction peak. The larger the crystals are, the higher the peak intensity. This supports the hypothesis that the lower the pH values, the larger the crystal size. Increasing the pH has already been shown to reduce crystallite size. The size of nanoparticles is affected by pH. The degree of crystallinity is correlated with the height and sharpness of the diffraction peaks. The ZnO NPs crystallinity increases with the diffraction peak's intensity. All samples achieved a high degree of crystallinity, according to the XRD characterization data; however, the ZnO sample produced at pH 8 produced the diffraction peak with the maximum intensity.

The XRD pattern showed no additional peaks that would have indicated the presence of contaminants or impurities, indicating the great purity of the produced compounds. The ZnO samples' diffraction peaks are broaden, suggesting that the samples had tiny particles and a high degree of crystallinity [14, 20]. It was discovered that every peak matched the standard's diffracted image quite well. The (101) reflection's intensity was significantly higher than the remaining ZnO peaks'. According to the XRD measurement, every ZnO peak was composed of the Wurtzite-shaped ZnO standard (JCPDS) file, similar Wurtzite-shaped ZnO was reported by Soumyadev *et al.* [14]. The XRD pattern has no additional peaks indicates that the sample is free of impurities and well crystallized which confirmed single phased crystalline structure of prepared ZnO nanoparticle. Similar result was reported by Ravi *et al.* [21]. The fine crystallite size of the ZnO particles is shown by the broad peaks in XRD patterns. Table 1 displayed the crystallite size and lattice constant of the structures derived from the XRD pattern. Using Eq. (1) and (2), the crystallite size and lattice constant were derived: The crystallite size and lattice constant of the structures generated from the XRD pattern were shown in Table 1. The crystallite size [22] and lattice constant were determined using Equation (1)

$$D = \frac{K\lambda}{\beta \cos\theta}, \tag{1}$$

$$\frac{1}{d^2} = \frac{h^2 + k^2}{a^2} + \frac{l^2}{c^2}, \tag{2}$$

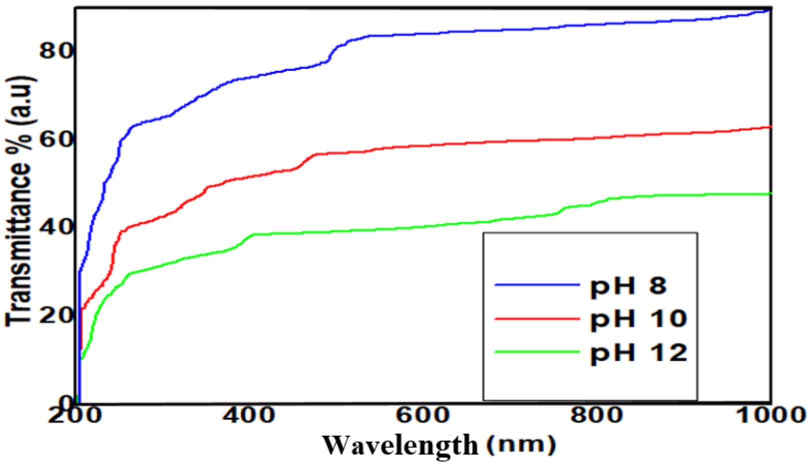

Figure 6. Transmittance spectral of ZnO nanoparticles at different pH.

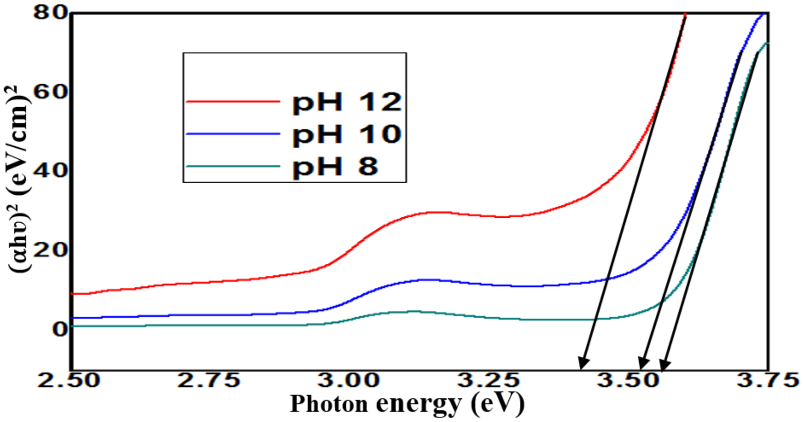

Figure 7. Optical energy band gap of ZnO NPs at different pH.

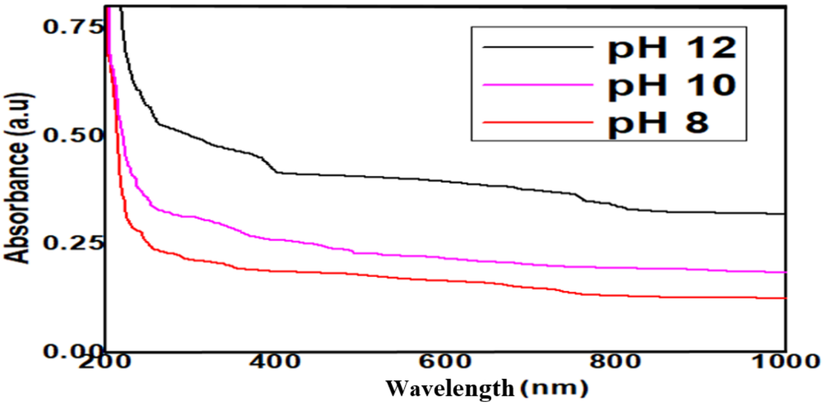

Figure 8. Absorption spectral of ZnO NPs at different pH.

$$\epsilon = \frac{\beta \cos\theta}{4}, \tag{3}$$

$$\delta = \frac{1}{D^2}, \tag{4}$$

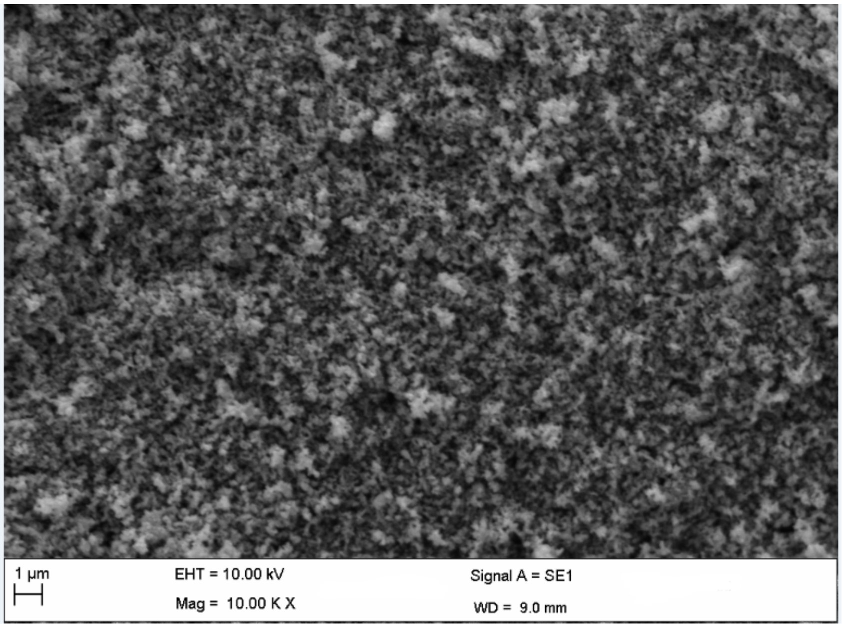

Figure 9. Surface morphology of ZnO nanoparticles at pH 12.

$$\rho_{\mathrm{XRD}} = \frac{\mathrm{CM}}{N_A a^3}, \tag{5}$$

where θ denotes the Bragg's diffraction angle, λ is wavelength of the X-ray, β is the full width at half maximum (FWHM), D is the size of the crystallite, a, c are the lattice constants and d is the distance between the planes that correspond to the Miller indices h, k, l. Table 1 displays the computed lattice constants and crystallite size at different alkaline pH. The results show that the lattice parameters increased from a value of a = 3.2553 Å for pH 8 to 3.2656 Å for pH 12, and from a value of c = 5.2245 Å for pH 8 to 5.2312 Å for pH 12, the changes in pH slightly increases proportionally. No considerable variation in the lattice characteristics at varying pH values is revealed. The computed lattice constants closely match the values reported in the literature. According to the literature, there is a direct correlation between particle size and the lattice parameter; that is, as particle size grows, the lattice parameter decreases [23]. High pH sample tends to exhibit higher lattice parameters due to the presence of defects and impurities. Such defects are introduced during sample preparation and vary according to method and reagents used.

The sharpness of the diffraction peaks indicates the presence of nanocrystalline domains inside the ZnO samples. Additionally, the narrow and sharp peaks verified the crystallization of the zinc oxide nanoparticles. When the pH is increased, the X-ray density drops due to an increase in the lattice parameter. Table 1 shows that the application of low pH, results in a decreased porosity due to large crystallite size. This porosity trend is understandable since that increasing pH causes the densities to fall and decrease the particle sizes, which in turn upturn the porosity. The dislocation density, which is determined by taking the reciprocal of square of the crystallite size of that peak, is commonly known as the length of dislocation lines per unit volume (lines/m^2) [24]. In crystal structure, the increase in dislocations and physical defects is caused by the presence of stress and strain forces. Therefore, the desolation density known as number of defects of the specimen and given in the Table 1. A low dislocation density is necessary for optimal crystallinity, and sample at low pH acquired low value is a proof of better crystallinity. The lowering value of dislocation density is obtained at low pH which enhances the particle size growth [24]. The internal micro strain was calculated using equation (4). The decrease in lattice defects along with the boundary level of the nanoparticles is indicated by micro strain, which reduced from 0.0547 to 0.0196 by decreasing the crystallite size. The d-spacing decreased as the diffraction angle increased at different lattice plane as shown in Table 2.

3.3. Optical characteristics

Figure 6 depicts the transmittance of ZnO NPs that were produced at various pH values. ZnO NPs produced at pH 8 show high percentage transparency in the visible as well as infrared parts of electromagnetic spectrum. When the particles are synthesized at pH 12, a low percentage transmittance of about 40% is created inside the visible area; when ZnO NPs is synthesized at pH 8, a huge percentage transmittance of relatively 85% is formed. At various pH levels of 8, 10, and 12, the percentage transmittance values of each sample are 85%, 58%, and 40%, respectively. Because a large number of optical charge carriers, or electrons, are created at pH 8 and add new energy levels to the energy band, the ZnO NPs synthesized at pH 8 exhibits improved transmittance. A larger percentage of transmittance is also a result of the increased population of charged particles and electron diffusion from the valence

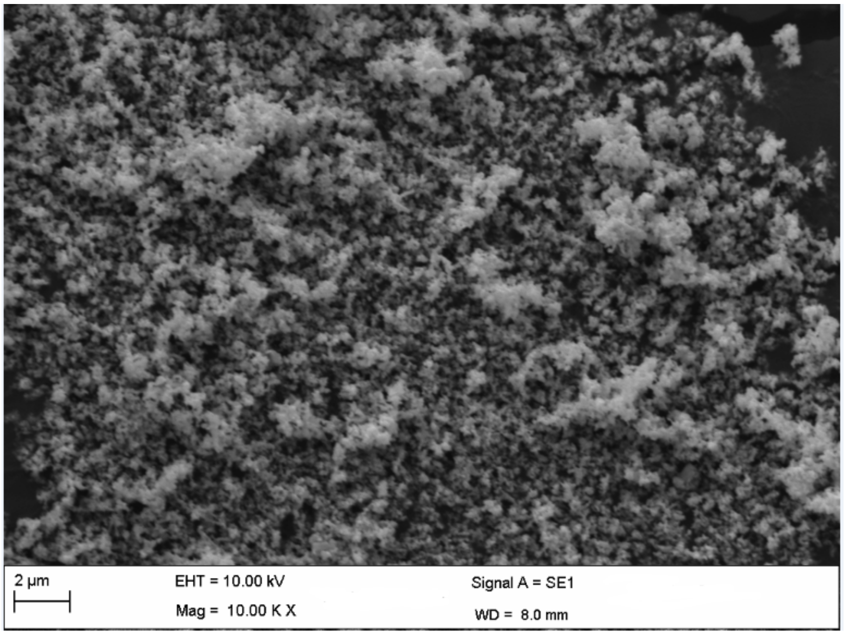

Figure 10. Surface morphology of ZnO nanoparticles at pH 10.

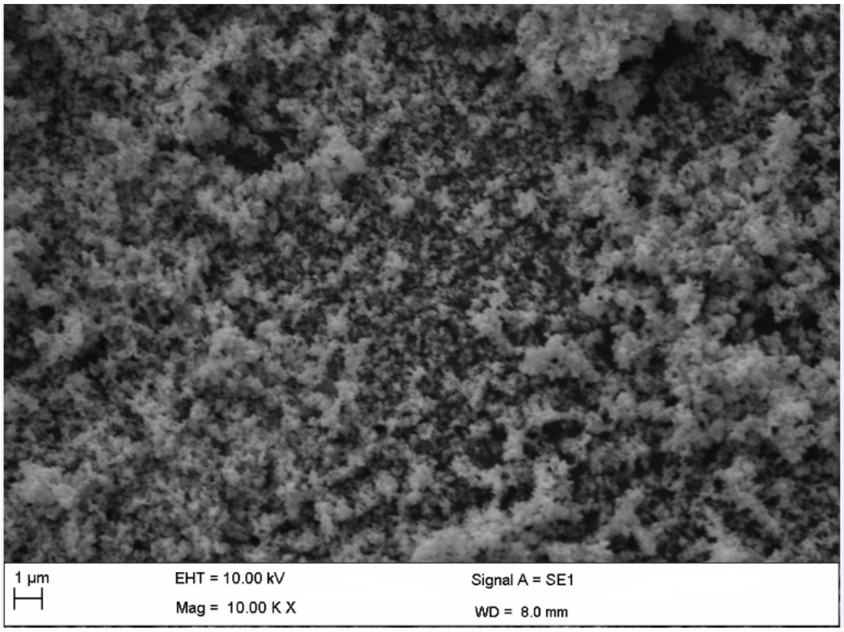

Figure 11. Surface morphology of ZnO nanoparticles at pH 8.

band to the conduction band [25, 26] in the sample synthesized at pH 8. The ZnO NPs that was synthesized at pH 8 is suitable for the development of efficient optoelectronic devices and may now be used to improve the fabrication of window layers for solar cell applications [27, 28]. The sample generated at a higher pH produces more optical loss, while the sample synthesized at a lower pH reveals a modest optical loss. For every sample, higher percentage transmittances are created in the infrared range. The results show that ZnO NPs are more transparent to infrared light, which opens the possibility of using ZnO to develop the perfect material for the detection of infrared radiation and can be mostly detected at low alkaline pH.

The Tauc analogy is based on energy-dependent absorption coefficient α which is represented by the equation (6): The approach for accurately calculating semiconductors' optical band gap energy using UV-Vis spectroscopy is Tauc method. The linear portion of the optical spectrum is typically directly extrapolated to the horizontal axis of the Tauc plot, $(\alpha h\upsilon)^n$ vs $h\upsilon$ to establish the appropriate band gap [29].

$$(\alpha h\nu) = A(h\nu - E_g)^n. \tag{6}$$

A is a constant, h is the Planck constant, υ is the photon's frequency, and Eg is the band gap's energy. Depending on the kind of electron transition, the n factor is either 1/2 for direct transition band gaps or 2 for indirect transition band gaps. Plotting $(\alpha h\upsilon)^n$ against photon energy (hυ) allows one to estimate the optical band gap energy for both direct and indirect transitions [30]. Extrapolating to $(h\alpha)^2 = 0$ for the direct transition yields the value of Eg. When the pH climbs from 8 to 12, the direct band gap decreases from 3.58 to 3.38 eV. These results are consistent with a prior work that discovered that as particle size decreases, the band gap expands [31]. The band gap of materials is directly impacted by the total concentration of ions, particularly H^+ and OH^-. In a charged conducting material, the electrons will have a close interaction with the counter ions of the solvation shell. The band gap of the material will be affected by the change in electron density brought about by the anion's approximation.

The energy band gap is obtained by extrapolating the linear path of the spectra lines as shown in Figure 7. The linear path of the spectra is extrapolated in order to evaluate the band gap energy. The band gap energy shifted between 3.38 to 3.58 eV, suggesting that variations in pH caused changes in the band gap. However, the physical state of ZnO changes when the pH of the alkaline solution is altered. When the pH is replaced, the energy band is shifted. A high band gap of around 3.58 eV is obtained during the synthesis of a ZnO sample synthesized at pH 8. The energy band gap for ZnO sample synthesized at pH 8, 10 and 12 are 3.58, 3.52 and 3.38eV, respectively. The blue shift, or chage in band gap energy from 3. 38eV to 3.58 eV, can be narrated using Burstein-Moss effect [32]. The band gap energy values make it clear that the nanoparticles exhibit a variety of optoelectronic uses, particularly when they are employed as solar cell window layers. The amount of optical absorption is highly dependent on the size of the particles; band gap energy values decrease as the particles get smaller, the particles get smaller as the pH rises. As a result, the particles dimension affects ZnO nanoparticles' capacity to absorb UV light. The huge band gap energy is the most important yardstick for ZnO application to optoelectronics [33]. For instance, Rao and Dutta [34] obtained a 4.7% conversion efficiency for dye-sensitized solar cells made of ZnO; additionally, ZnO with an Eg value of 3.2 eV have been employed as DSSC working electrode which is recognized as a material worthy to be substituted with TiO_2 based DSSC working electrode [35]. The properties of ZnO are influenced by its diverse characterizations at different pH values. Meanwhile, the conversion efficiency can be increased using ZnO sample that has band gap energy greater than 3.2 eV.

The absorption bands created by ZnO nanoparticles are displayed in Figure 8. UV light was significantly absorbed by ZnO sample synthesized at pH 12. The outcomes demonstrated that the high transmittance of ZnO nanoparticles synthesized at alkaline pH 8 to photon energy led to low absorption. The absorbance of the sample synthesized at pH 12 is higher than the sample synthesized at pH 8 and 10. ZnO samples that show an elevated optical absorption edge in the ultraviolet spectrum can be used appropriately with UV detectors. Saleem *et al.* [24], Anjum *et al.* [36], and Arshad *et al.* [37] all reported results that were similar. Subsequently that it absorbs, detects, and filters UV radiation that is capable of causing interior home systems to heat up, ZnO nanoparticles synthesized at pH 12 is now an excellent choice for UV photodetector and for checking and controlling UV in architectural windows. This material's strong absorption within the ultraviolet region makes it a prominent compound for efficient UV radiation control. According to the absorbance, all of the materials showed strong absorbance values in the UV range, which sharply decreased as they approached the NIR range.

ZnO's light absorption is greatly enhanced at high pH levels, making it a viable photovoltaic material. It was discovered that adding pH 12 increases the absorption rates of ZnO and the absorbance value was dramatically raised. Imosobomeh *et al.* [20] demonstrated a similar outcome, stating that the addition of molybdenum to cerium telluride increases the absorption rates of cerium telluride. As a result, cerium telluride doped molybdenum is now a viable option for solar applications [38]. ZnO material showed strong absorbance values in the UV–Vis area, which sharply decreased as they moved towards the NIR region, according to the absorbance of ZnO at pH 12. It was found that adding pH 12 to the precursors significantly increased the absorbance value, indicating that the ZnO's light absorption was much enhanced, making it a suitable PV material. Imosobomeh *et al.* [20] obtained a similar outcome, showing that doping ZnO with erbium significantly increased its light absorption, making it a promising photovoltaic material [39]. Furthermore, because of its high absorption, ZnO has been shown to be beneficial as an energy storage material when doped with graphene particles [40].

3.4. Surface morphology of samples

SEM was adopted in examining the microstructural characteristics of ZnO nanoparticles. Grain size and surface roughness were examined. The SEM images of ZnO crystalline structure at pH values of 8, 10 and 12 were displayed in Figures 9-11. According to a detailed SEM micrograph study, it appeared quite dense and free of cracks. On SEM pictures, porosity and grain growth pattern were clearly seen. The grain distribution is heterogeneous, and some of the sizes were slightly larger. The images appeared smooth and front-oriented, and the grain size of the synthesized sample, as determined by SEM results, are 18 nm, 31 nm and 35 nm at pH 12, 10 and 8. As the effect of the pH values upsurging for all samples, the grain size grows at pH 8, but at pH 10 and 12, the grain size drops. The samples are cloudy and were found to be moderately compacted and free of cracks after a comprehensive SEM micrograph investigation. On SEM pictures, porosity and the grain growth patterns were clearly visible. At pH 8, Figure 11 exhibits surface roughness and shows the development of heterogeneous tightly packed structure and spongy-like nano-grains with porosity; nonetheless, the compactness and densely packed nature appear to be affected by pH change. Homogeneity at the surface layer is shown by the lack of surface defects like voids at the surface morphology. When compared to a sample prepared at pH 12, the morphology is likewise uniform, with spongy-like and spherical grains that are compacted and firmly packed, but with less grain growth. Grain growth is less in the ZnO sample synthesized at pH 12 than in the sample created at pH 10 and 8, but the surface morphology of the ZnO sample synthesized at pH 12 showed the presence of homogeneity at the surface layer and the absence of surface flaws such pores, holes, and cavities. There was evidence of particle aggregation based on the surface configuration at pH 8. ZnO sample agglomeration is a process that reduces free surface energy by increasing particle size and decreasing surface area. The adherence of ZnO nanoparticles to each other by weak forces causes agglomeration.

The morphologies show the appearance of high density packed structure and significant compactness at all pH values. Because of the lack of contaminants and non-distortion at the lattice site, the ZnO sample synthesized at pH 12 showed little or no aggregation. The sample synthesized at pH 12 were homogeneous across a vast surface area and had smaller crystalline grains than other samples and cloud-like morphology revealed at low pH values is reduced. While the cloud-like structure has a homogeneous distribution of grains and modest porosity, the cloud-like morphology in the current investigation showed a homogeneous distribution of particles. The smooth and uniform shape of sample synthesized at pH 12 with large-scale homogeneity is an important point: it suggests that these nanoparticles may be useful for photo-detectors [24]. The agglomeration that was present in the sample synthesized at pH 8 was reduced at pH 10 which disappear at pH 12, according to the SEM images. Both specimens at pH 10 and 8 showed evidence of particle aggregation, which might be related to their crystalline sizes. The grains cannot grow because of the agglomeration. The increased surface energy caused by the nanoparticles' greater surface area to volume is reduced by their ability to agglomerate. The increase of pH of the synthesized samples in alkaline medium in the current work reduces agglomeration, which raises surface energy since the surface area to volume ratio is reduced. The use of pH 12 leads to the formation of heterogeneous nucleation sites and growth, which together reduce agglomeration. The reduced agglomeration of the nano-crystallites increases the surface area and decreases the internal microstrain. Additionally, we found that the use of pH 12 increased the sample's compactness, smoothed out its structures, and determined the orientation of the nanoparticles. The specimen's microstructure varies as a result of pH variation. Therefore, it can be said that the use of pH 12 significantly enhances the surface characteristics of the nanoparticles, which may lead to better photosensing. Altering the reaction system's pH values allowed for the control of the nanoparticles' size. Smaller nanoparticles were produced at higher pH values than at lower pH levels. The variation in the precursor's rate of decrease is the cause of this discrepancy. Similar result was reported by Alqadi et al who reported smaller silver nanoparticles at high pH [41].

4. Conclusion

The co-precipitation approach was utilized to successfully manufacture ZnO NPs in alkaline solution at pH 8, 10 and 12. The (101) reflection plane is the optimal orientation for the creation of wurtzite-hexagonal structure and ZnO phase, according to the XRD study. ZnO synthesized at pH 8, 10 and 12 have crystallite diameters of 29.74, 17.83 and 12.64 nm in that order. The ZnO sample synthesized at pH 8 shows the best optical features due to its strong optical gain, while the sample of ZnO synthesized at pH 12 shows optical losses. It has been noted from this work that varying the pH of the precursor modified the zinc oxide sample for various industrial applications. For instance, the use of pH 12 significantly increased the absorbance value, indicating that ZnO's light absorption is significantly enhanced at high pH levels, making it a promising photovoltaic material and ultraviolet detector. Meanwhile, the addition pH 8 significantly increased the transmittance value, indicating that ZnO's visible light transparency is significantly enhanced at low pH levels in alkaline medium, making it a promising optoelectronics material and active infrared detector. The results from this research show that zinc oxide can be used as optoelectronics, photovoltaic material, infrared and ultraviolet detectors.

Data Availability

No additional data was used beyond those presented in the submitted manuscript.

References

[1] I. L. Ikhioya, E. U. Onoh, A. C. Nkele, B. C. Abor, B. C. N. Obitte, M. Maaza & F. I. Ezema, "The green synthesis of copper oxide nanoparticles using the moringa oleifera plant and its subsequent characterization for use in energy storage applications", East Eur. J. Phys. **1** (2023) 162. https://periodicals.karazin.ua/eejp/article/view/21046.

[2] S. O. Samuel, M. L. Frank, E. P. Ogherohwo, A. Ekpekpo, J. T. Zhimwang & I. L. Ikhioya, "Influence of deposition voltage on strontium sulphide doped silver for optoelectronic application", East Eur. J. Phys. **1** (2023) 189. https://periodicals.karazin.ua/eejp/article/view/21094.

[3] I. L. Ikhioya, U. O. Faith & I. U. Courage, "Impact of modulated temperature on photovoltaic properties of automated spray fabricated zirconium doped cobalt selenide films", Mater. Res. Innov. **27** (2023) 382. https://www.tandfonline.com/doi/abs/10.1080/14328917.2023.2178747.

[4] I. L. Ikhioya, U. O. Edwin, N. O. Donald & J. E. Azubuike, "Impact of bismuth as dopant on ZnSe material syntheses for photovoltaic application", Mater. Res. Innov. **27** (2023) 411. https://www.tandfonline.com/doi/abs/10.1080/14328917.2023.2180582.

[5] L. I. Imosobomeh, I. A. Nwamaka & F. U. Ochai-Ejeh, "Influence of erbium (Er) dopant on the enhanced optical properties of electrochemically deposited zinc oxide (ZnO) films for high-performance photovoltaic systems", Optik **252** (2022) 168486. https://www.sciencedirect.com/science/article/abs/pii/S0030402621019872.

[6] R. Dutta, S. Chattopadhyay, A. Sarkar, M. Chakrabarti, D. Sanyal & D. Jana, "Role of defects in tailoring structural, electrical and optical properties of ZnO", Progress in Materials Science **54** (2009) 89. https://www.sciencedirect.com/science/article/abs/pii/S0079642508000698.

[7] A. Ali, A. Nadiah, T. Ter, J. Hidayani, A. Syamsir & M. L. Rahimi. "Optical and Structural Properties of Controlled pH Variation on Zinc Oxide Nanostructured via Hydrothermal Method", Key Engineering Materials **908** (2022) 253. https://doi.org/10.4028/p-w3o207.

[8] P. K. Giri, S. Bhattacharyya, Dilip K. Singh, R. Kesavamoorthy, B. K. Panigrahi & K. G. M. Nair, "Correlation between microstructure and optical properties of ZnO nanoparticles synthesized by ball milling", Journal of Applied Physics **102** (2007) 093515. https://cir.nii.ac.jp/crid/1362262946454599936.

[9] S. Ghosh, A. Ghosh, S. Pramanik, K. K. Probodh, R. Sen & S. K. Neogi. "Synthesis of ZnO nanoparticles by co-precipitation technique and characterize the structural and optical properties of these nanoparticles", Journal of Physics: Conference Series. **2349** (2022) 012014. https://iopscience.iop.org/article/10.1088/1742-6596/2349/1/012014/meta.

[10] l. Tereshchenko, M. Bechelany, R. Viter, V. Khranovskyy, V. Smyntyna, N. Starodub & R. Yakimova. "Optical biosensors based on ZnO nanostructures: advantages and perspectives", A review, Sensors and Actuators B: Chemical **229** (2016) 664. https://www.sciencedirect.com/science/article/abs/pii/S0925400516300995.

[11] S. Ghosh, G. Khan, B. Das & K. Mandal. "Defect-driven magnetism in luminescent n/p-type and Gd-substituted SnO$_2$ nanocrystalline thin films", Journal of Applied Physics **109** (2011) 123927. https://pubs.acs.org/doi/abs/10.1021/am300023a.

[12] R. Baghdad, B. Kharroubi, A. Abdiche, M. Bousmaha, M. A. Bezzerrouk, A. Zeinert, M. El Marssi, K. Zellama, "Mn doped ZnO nanostructured thin films prepared by ultrasonic spray pyrolysis method", Superlattices and Microstructures **52** (2012) 711. https://www.sciencedirect.com/science/article/abs/pii/S0749603612001875.

[13] S. K. Neogi, A. M. Ahmed, A. Banerjee & S. Bandyopadhyay, "Enhanced ferromagnetism by ion irradiation for substitutionally cobalt doped ZnO films", Applied Surface Science **481** (2019) 443. https://www.sciencedirect.com/science/article/abs/pii/S0169433219307731.

[14] G. Soumyadev, G. Abhishek, P. Subhamay, K. K. Probodh, S. Rupam & K. N. Swarup, "Synthesis of ZnO nanoparticles by co-precipitation technique and characterize the structural and optical properties of these nanoparticles", Journal of Physics: Conference Series **2349** (2022) 012014. https://doi.org/10.1088/1742-6596/2349/1/012014.

[15] A. H. Zyoud, A. Zubi, S. H. Zyoud, M. H. Hilal, S. Zyoud, N. Qamhieh, A. Hajamohideen & H. S. Hilal, "Kaolin-supported ZnO nanoparticle catalysts in self-sensitized tetracycline photodegradation: Zero-point charge and pH effects", Appl. Clay Sci. **182** (2019) 105294. https://www.sciencedirect.com/science/article/abs/pii/S0169131719303527.

[16] N. P. Shetti, S. J. Malode, D. S. Nayak, G. B. Bagihalli, S. S. Kalanur, R. S. Malladi, C. V. Reddy, T. M. Aminabhavi & K. R. Reddy, "Fabrication of ZnO nanoparticles modifed sensor for electrochemical oxidation of methdilazine", Appl. Surf. Sci. **496** (2019) 143656. https://www.sciencedirect.com/science/article/abs/pii/S0169433219324535.

[17] S. Arya, P. Mahajan, S. Mahajan, A. Khosla, R. Datt, V. Gupta, S. J. Young, S. K. Oruganti, "Review—Infuence of Processing Parameters to Control Morphology and Optical Properties of Sol-Gel Synthesized ZnO Nanoparticles", ECS J. Solid State Sci. Technol. **10** (2021) 23002. https://iopscience.iop.org/article/10.1149/2162-8777/abe095/meta.

[18] N. F. Khairol & N. Sapawe, "Electrosynthesis of ZnO nanoparticles deposited onto egg shell for degradation of Congo red", Mater. Today Proc. **5** (2018) 21936. https://www.sciencedirect.com/science/article/abs/pii/S2214785318318522.

[19] V. Koutu, S. Shastri & M. M. Malik, "Effect of NaOH concentration on optical properties of zinc oxide nanoparticles", Materials Science Poland **34** (2016) 819. https://yadda.icm.edu.pl/baztech/element/bwmeta1.element.baztech-a44d6897-759d-463c-bc5e-d84df744132f.

[20] L. I. Imosobomeh & C. N. Agnes, "Properties of electrochemically-deposited NiTe films doped with molybdenum at varying temperatures", Results in Optics **12** (2023) 100494. https://www.sciencedirect.com/science/article/pii/S2666950123001463.

[21] R. Ravi, K. K. Choudhary & K. Netram. "The Structural and Optical Properties of Zinc-Oxide Nanomaterials Synthesized via Thermal Decomposition Method", Journal of Physics: Conference Series **2603** (2023) 012003. https://iopscience.iop.org/article/10.1088/1742-6596/2603/1/012003/meta.

[22] R. J. Peverga, M. C. Khaled, Y. Yushamdan, A. Nathan-Abutu , V. M. Igba, E. Danladi, O. S. Obaseki, M. B. Ochang, W. V. Zhiya & F. K. Yam, "An Alternative Method for Estimating the Phase Fraction of Multiphase Nanomaterials: Analysis from X-ray Diffraction", Journal of Applied Sciences and Nanotechnology **3** (2023) 1222. https://doi.org/10.53293/jasn.2023.7002.1222.

[23] V. N. Morris, R. A. Farrell, A. M. Sexton & M. A. Morris, "Lattice Constant Dependence on Particle Size for Ceria prepared from a Citrate Sol-Gel", Journal of Physics: Conference Series **26** (2006) 119. https://iopscience.iop.org/article/10.1088/1742-6596/26/1/028/meta.

[24] S. Saleem, M. N. Ashiq, S. Manzoor, U. Ali, R. Liaqat, A. Algahtani, S. Mujtaba, V. Tirth, A. M. Alsuhaibani, M. S. Refat, A. Ali, M. Aslam, A. Zaman, "Analysis and characterization of opto-electronic properties of iron oxide (Fe$_2$O$_3$) with transition metals (Co, Ni) for the use in the photodetector application", Journal of materials research and technology **25** (2023) 6150. https://www.sciencedirect.com/science/article/pii/S2238785423015934.

[25] U. Baishya & D. Sarkar, "Structural and optical properties of zinc sulphide-polyvinyl alcohol (ZnS-PVA) nanocomposite thin films: effect of Zn source concentration", Bull Mater Sci **34** (2011) 1285. https://link.springer.com/article/10.1007/s12034-011-0316-9.

[26] S. A. Mansour, F. Yakuphanoglu, "Electrical-optical properties of nanofiber ZnO film grown by sol gel method and fabrication of ZnO/p-Si heterojunction", Solid State Sciences **14** (2012) 12. https://www.sciencedirect.com/science/article/abs/pii/S129325581100344X.

[27] A. A. Ibiyemi, G. T. Yusuf, O. Olubosede, A. Olusola & H. A. Akande, "x-ray photoelectric and magnetic properties of chemically synthesized Cd–Ni Ferrite nanomagnetic particles", Physica Scripta **97** (2022) 025804. https://iopscience.iop.org/article/10.1088/1402-4896/ac4a95/meta.

[28] G. Bachir, S. L. Eddine, M. Souhaila, B. Abderrhmane, H. Hadia, L. T. Mohammed, T. Gobika, B. Ahmed & M. Farid. "Effect of pH Value on the Band gap Energy and Particles Size for Biosynthesis of ZnO Nanoparticles: Efficiency for Photocatalytic Adsorption of Methyl Orange". Sustainability **14** (2022) 11300. https://www.mdpi.com/2071-1050/14/18/11300.

[29] R. J. Peverga, E. Danladi, U. I. Ndeze, O. Adedokun, S. Landi, A. J. Haider, A. T. Adepoju, Y. Yusof, O. S. Obaseki & F. K. Yam, "Comment about the use of unconventional Tauc plots for bandgap energy determination of semiconductors using UV–Vis spectroscopy", Results in Optics **14** (2024) 100606. https://www.sciencedirect.com/science/article/pii/S2666950124000038.

[30] A. Bouafia, S. E. Laouini, M. LTedjani, G. A. M. Ali & A. Barhoum, "Green biosynthesis and physicochemical characterization of Fe$_3$O$_4$ nanoparticles using Punica granatum L. fruit peel extract for optoelectronic applications", Text. Res. J. **92** (2022) 685. https://journals.sagepub.com/doi/abs/10.1177/00405175211006671.

[31] S. A. Kulkarni, P. S. Sawadh, P. K. Palei & K. K. Kokate, "Effect of synthesis route on the structural, optical and magnetic properties of Fe3O4 nanoparticles". Ceramics International **40** (2014) 1945. https://doi.org/10.1016/J.ceramint.2013.07.103.

[32] P. P. Hankare, R. P. Patil, A. V. Jadhav, R. S. Pandav, K. M. Garadkar, R. Sasikala & A. K. Tripathi, "Synthesis and characterization of nanocrystalline Ti-substituted Zn ferrite", Journal of Alloys Compound **509** (2011) 2160. https://www.sciencedirect.com/science/article/abs/pii/S0925838810027039.

[33] S. J Pearton, D.P. Norton, K. Ip, Y.W. Heo & T. Steiner, "Recent progress in processing and properties of ZnO, Superlattices and Microstructures", **34** (2003) 3. https://www.sciencedirect.com/science/article/abs/pii/S0749603603000934.

[34] A.R. Rao & V. Dutta, "Achievement of 4.7% conversion efficiency in ZnO dye-sensitized solar cells fabricated by spray deposition using hydrothermally

synthesized nanoparticles", Nanotechnology **19** (2008) 445712. https://iopscience.iop.org/article/10.1088/0957-4484/19/44/445712/meta.

[35] G. Boschloo, T. Edvinsson, A. Hagfeldt (Eds.), "Dye-sensitized Nanostructured ZnO Electrodes for Solar Cell Applications. Handbook of Nanostructured Materials for Solar Energy Conversion", In *Nanostructured materials for solar energy conversion*, Elsevier, 2006, pp. 227–254. https://www.sciencedirect.com/science/article/abs/pii/B9780444528445500093.

[36] S. Anjum, T. Zeeshan, M. Danish Ali, S. Waseem, I. Waseem & Z. Mustafa, "Investigation of cationic distribution, Y–K angles & optical and dielectric properties of as-synthesized cerium-doped cobalt nano-ferrites prepared by co-precipitation method", Applied Physics A **128** (2022) 383. https://doi.org/10.1007/s00339-022-05470-8.

[37] S. Arshad, A. Hussain, S. Noreen, N. Bibi, M. B. Tahir, J. Rehman, M. Jabeen, H. Benish Munawar & S. Rahman, "Structural, mechanical, electronic and optical properties of MFe_2O_4 (M=Zn, Cu, Si) ferrites for electrochemical, photocatalytic and optoelectronic applications", Journal of Solid State Chemistry **330** (2024) 124504. https://www.sciencedirect.com/science/article/abs/pii/S0022459623006722.

[38] L. I. Imosobomeh, O. A. Samson, A. A. Ishaq & I. E. Fabian, "The effect of molybdenum dopant on rare earth metal chalcogenide material", Chemical Physics Impact **7** (2023) 100269. https://www.sciencedirect.com/science/article/pii/S2667022423001093.

[39] I. L. Imosobomeh, I. A. Nwamaka & U. O. Faith, "Influence of erbium (Er) dopant on the enhanced optical properties of electrochemically deposited zinc oxide (ZnO) films for high-performance photovoltaic systems", Optik **252** (2022) 168486. https://www.sciencedirect.com/science/article/abs/pii/S0030402621019872.

[40] I. Ahmad, A. Shakoor, W. Ahmad, A. Hussain, A. S. Iftikhar & I. L. Ikhioya, "The impact of zinc ions on electrode material for energy storage in solvothermal-synthesised graphene-zinc oxide nanocomposites", Materials Research Innovations **29** (2024) 117. https://www.tandfonline.com/doi/abs/10.1080/14328917.2024.2387404.

[41] M. K. Alqadi, O. A. Abo Noqtah, F. Y. Alzoubi, J. Alzouby & K. Aljarrah "pH effect on the aggregation of silver nanoparticles synthesized by chemical reduction", Materials Science-Poland **32** (2014) 107. https://link.springer.com/article/10.2478/s13536-013-0166-9.